19th Brazilian Congress of Thermal Sciences and Engineering
November 6th–10th, 2022, Bento Gonçalves - RS - Brazil

ENC-2022-0377
EXPERIMENTAL STUDY OF THE CAVITATION ON BIO-INSPIRED HYDROFOILS WITH LEADING-EDGE PROTUBERANCES

Arthur Augusto Alves
Henrique Matos Campos
Aluisio Viais Pantaleão
Department of Mechanical Engineering, School of Engineering, São Paulo State University (Unesp), Brazil
arthur.a.alves@unesp.br, hmatoscampos@gmail.com, aluisio.pantaleao@unesp.br

Abstract. *Devices that suffer from cavitation can have their lifetime and efficiency decreased. A possible alternative found in the literature to mitigate the cavitation is the use of bio-inspired devices such as leading-edge protuberances. It was verified that the protuberances can increase the lift and reduce the cavitation in specific conditions. So, we investigated, in an experimental work, the possibility of mitigating the cavitation in hydrofoils with leading-edge protuberances. The models analysed are the baseline and two kinds of sinusoidal leading-edge geometries (protuberances) called 4S and 4M. The experimental methodology involved flow visualisation techniques in the vertical hydrodynamic tunnel. The flow was registered by a camera in a range of 2° to 14° of angle of attack and for a Reynolds number up to approximately* 2×10^4*. After recording the possible incipient cavitation, a high-speed camera was used in a deeper investigation of the best conditions. It was observed a tendency for bubbles to appear in lower Reynolds numbers with the increase of the angle. At an angle of 8°, a significant mitigation of bubbles in the 4S foil is noticeable compared to the other models under the same conditions. Additionally, it was obtained, with the high-speed camera, a detailed visualisation of the incipient cavitation on these bio-inspired hydrofoils that allowed to record more precisely the occurrence of coalescence and the origin of the adhered bubbles. The results obtained can be used as a benchmark in numerical simulation research.*

Keywords: *Hydrofoil; cavitation; bio-inspired; leading-edge protuberances; high-speed camera.*

1. INTRODUCTION

A lot of engineering solutions are inspired by nature, with this premise, bio-inspired hydrofoils with leading-edge protuberances have been receiving increasing attention in recent years. These hydrofoils are inspired by the pectoral fins of humpback whales (Megaptera novaeangliae) as can be seen in the Figure 1. This whale species is particularly agile, capable of performing rolls and loops underwater (Van Nierop *et al.*, 2008).

Fish and Battle (1995) characterised the hydrodynamic design of pectoral fins of humpback whales, highlighting the similarity of their cross section with aerodynamic profiles and emphasising the presence of protuberances. In addition to characterisation, the authors chose the NACA $63_4 - 021$ airfoil as the baseline and suggested that the improved hydrodynamic performance may be associated with the protuberances that, possibly, have the function of improve lifting devices to control and maintain lift at high angles of attack.

Johari *et al.* (2007) performed experiments in a hydrodynamic tunnel with a Reynolds number of approximately 1.83×10^5 using the baseline NACA $63_4 - 021$ profile and 6 other variations with protuberances on the leading edge. They found that the protuberances influenced parameters such as drag and lift coefficients. For angles of attack smaller than the baseline stall angle, lift reduction and drag increase were observed for the modified foils. With angle above the stall angle, an improvement of up to 50%, with little or no drag penalty, was obtained in the lift coefficient of modified foils compared to baseline under specific conditions.

Hansen *et al.* (2016) investigated, through experimental and numerical studies, the formation and evolution of streamwise vortices produced by the protuberances on a NACA 0021 foil at Reynolds number of 2230. Their experimental results demonstrate that the flow characteristics pressure gradients near the leading edge vary with time, particularly near the trailing edge and at a higher angle of attack. Furthermore, the numerical investigation revealed that the foil with protuberances is slightly better than the unmodified.

In order to qualitatively analyse the phenomenon of cavitation in the same profiles, Johari (2015) photographed each

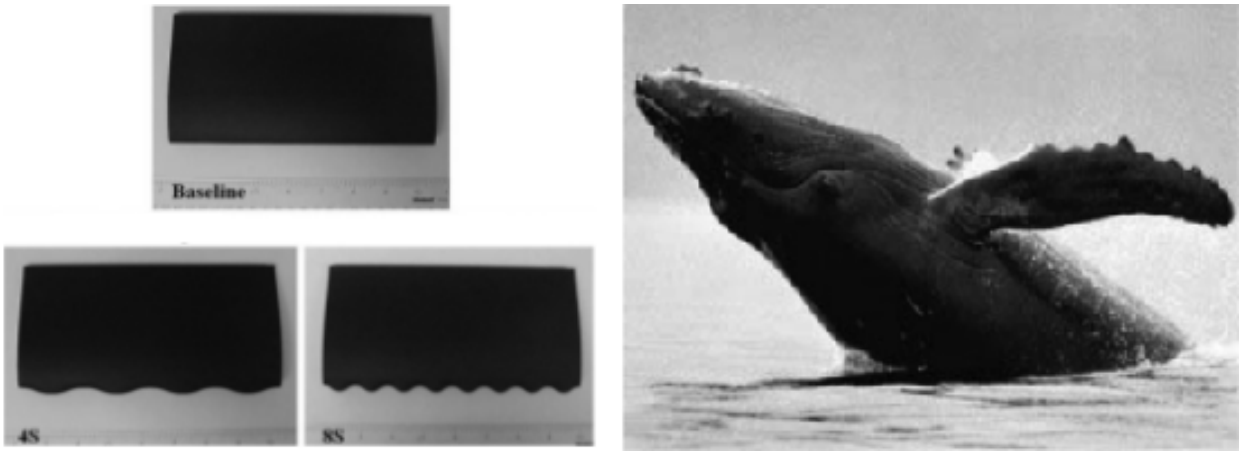

Figure 1. Bio-inspired hydrofoils and the pectoral fins of a humpback whale. Available from: Johari *et al.* (2007).

hydrofoil under a Reynolds number flow of 7.2×10^5, with an angle of attack from 12º to 24º. According to the results, incipient cavitation formation started to occur at smaller angles in the profiles with protuberances than in the baseline. This early formation occurred in the valleys of the protuberances. At high angles of attack, the cavitation was concentrated behind the valleys, while at baseline the cavitation was present in almost every leading edge. In profiles with higher protuberances amplitudes (4L and 4M) cavitation was notably restricted to valleys.

With a similar premise to Johari (2015), but to analyse quantitatively, force measurements were carried out by Custodio *et al.* (2018) using a waterproof load cell, and cavitation patterns were recorded by directly imaging the hydrofoil NACA $63_4 - 021$ surface. They verified that cavitation on the modified hydrofoils, mostly on two larger amplitudes (called 4M, 4L, 8M and 8L), was mainly confined to the regions behind the protuberance troughs. Additionally, cavitation on the modified hydrofoils appeared at lower angles of attack than on the baseline model. Li *et al.* (2020) conducted numerical studies also to investigate cavitation in the modified profiles and obtained results similar to the results of Custodio *et al.* (2018). Furthermore, the authors obtained parameters that confirm the alteration of the pressure field on the profile as a consequence of the presence of protuberances, altering the position and the extent of the cavitation.

Li *et al.* (2021a) and Li *et al.* (2021b) used numerical methods for the analysis of hydrodynamic profiles also inspired by pectoral fins of humpback whales and obtained favourable findings for bio-inspired profiles. Li *et al.* (2021a) obtained results that indicated that the modified leading edge can improve lift-drag characteristics, restrict hydrofoil cavitation and reduce cavitation volume by approximately 30%. In addition, they found that increasing the amplitude of the leading-edge ripple can reduce the pressure amplitude by approximately 60%, significantly reducing the volume of cavitation. Li *et al.* (2021b) found that the protuberances act as vortex generator, continuously influencing the vorticity in the boundary layer, improving the hydrodynamics of the hydrofoil, delaying separation and weakening the scale of cavitation.

The purpose of this work was to investigate the possibility of mitigating the cavitation in hydrofoils with leading-edge protuberances. The models investigated are the baseline, 4S and 4M that were used by Johari *et al.* (2007). The experimental methodology involved flow visualisation techniques in the vertical hydrodynamic tunnel. The flow was registered by a camera in a range of 2° to 14° of attack angle and in a Reynolds number up to approximately 2×10^4. The study also aimed to thoroughly investigate the origin and the adherence of the bubbles, also other possible phenomena that are affected by the protuberances and are too fast to be analysed without the high-speed camera.

2. METHODOLOGY

2.1 Vertical Hydrodynamic Tunnel

Hydrodynamic tunnels have constructive and operational simplicity, and their main advantage is the use of liquid as a working fluid which promotes easier visualisation of the flow. According to Lindquist (1999), the acquisition of high-definition flow images makes this type of installation an excellent working tool for research development and for didactic applications. So, vortices, recirculations, jets, wakes and detachments can be made visible with great sharpness and clarity using dispersed solid particles ink streams injected into the flow or small gas bubbles suspended in the free stream.

The tunnel used has the singularity of having a vertical configuration that guarantees advantages in the analysis of cavitation, allowing a clear and accessible visualisation of the flow in the 4 side views of the test section. A illustration of the vertical hydrodynamic tunnel used is shown in Figure 2.

The tunnel consists of an upper reservoir (UR) equipped with netting and honeycomb (NC) to get a laminar flow. There is a contraction (CT) and, after that, the test section (TS) where the hydrofoil (HF) is fixed. The tunnel is filled up by the supply system (SS) that directs the water from the lower reservoir (LR) to the upper reservoir (UR). The supply

valve (SV) controls the supply. Another valve after the flow meter (FM) controls the outlet that allows the water back to the lower reservoir (LR).

The test section where the hydrofoil is fixed has dimensions of 146 x 146 mm with the ends trimmed, being 500 mm long. The matrix that composes the section is made of aluminum and has four acrylic windows.

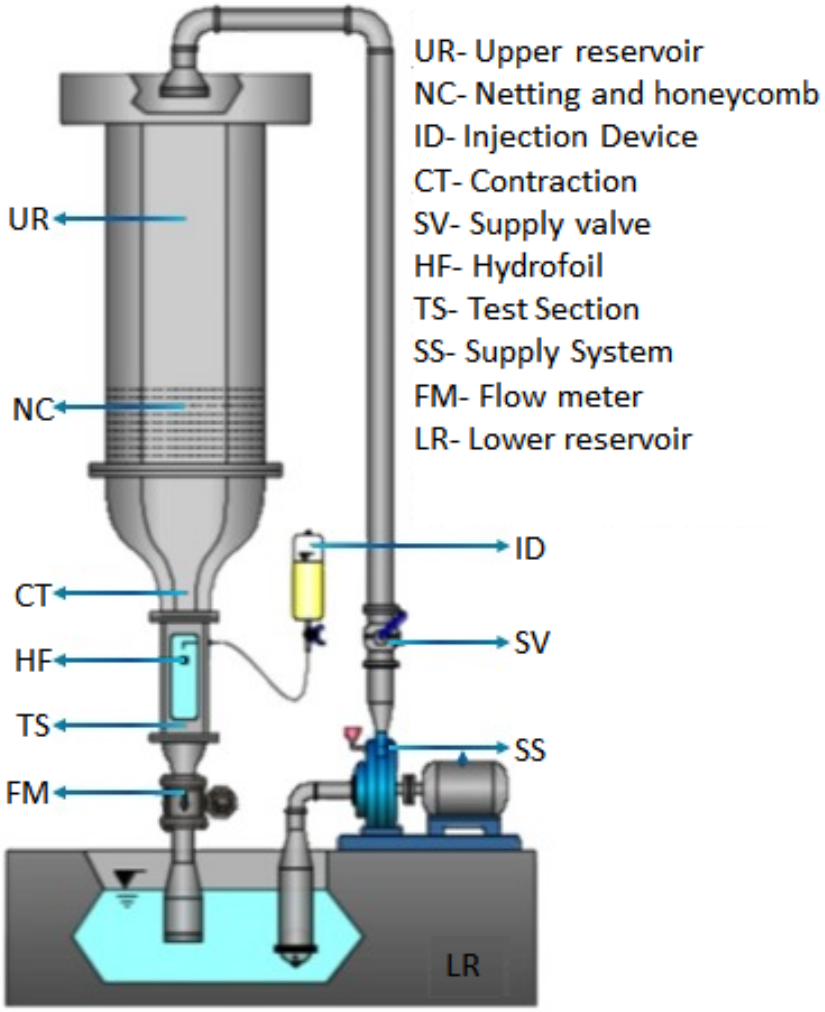

Figure 2. Vertical Hydrodynamic Tunnel representation. Adapted from: Bassan (2011).

2.2 Models

The models investigated, as Johari *et al.* (2007), are the baseline (NACA $63_4 - 021$) and two kinds of sinusoidal leading edge geometries (protuberances) that were defined by a wavelength of 50% of the NACA $63_4 - 021$ mean chord length and two amplitudes of 2.5% and 5% of the NACA $63_4 - 021$ mean chord length being, respectively, the models 4S and 4M.

Salome, a computer-aided design *software* (CAD - *Computer-aided Design*), was used to design the models, which were 3D printed through the MakerBot Replicator Plus 3D printer using the PLA filament. After printing, a surface treatment was required to eliminate the inherent roughness of 3D printing, so the models were softly sanded to eliminate roughness and maintain the same shape.

2.3 Procedure

The first tests performed were with baseline, as its results would be used as a reference for tests with the modified leading edge. The methodology consisted of increasing the flow rate until the formation of the first bubbles and then recording the Reynolds number and pictures of the flow. Then, the flow rate was increased until reaching approximately Reynolds number of 20,000. During this increase, pictures and the respective Reynolds numbers were recorded when there was a significant change in the quantity and characteristics of the bubbles. This procedure was executed in the same

way for the angles of attack of 2°, 8° and 14°, so that the data obtained would be the reference for the tests with the 4S and 4M foils. Similarly, the tests with the 4S and 4M foils were performed with the same procedure, and the records were made, mainly, under the same conditions registered in the baseline in order to compare them. After to record the pictures using a Nikon D90 camera, the same procedure was made with a Photron high-speed camera model FASTCAM SA3 60K M3 for the chosen conditions, recording 1000 frames per second for a deep investigation.

2.4 Flow Rate

The flow rate was controlled by a valve and measured by the magnetic flow meter (FM) of the brand Yokogawa model ADMAG AE208MG. With the value obtained, the free current speed can be calculated. Equation 1 demonstrates the calculation of the free current velocity.

$$U = \frac{Q}{A} \tag{1}$$

where U is the free flow rate velocity, Q is the volumetric flow rate and A is the cross-sectional area of flow on TS section.

Most phenomena in fluid mechanics show complex dependence on geometric and flow parameters. Therefore, it is necessary to use dimensionless numbers for a better analysis of such phenomena. In this work, the flow analysis was performed as a function of the Reynolds number, Equation 2.

$$Re = \frac{\rho U L}{\mu} \tag{2}$$

where L is the NACA $63_4 - 021$ aerodynamic mean chord, ρ is the fluid density and μ is the fluid dynamic viscosity.

3. RESULTS

The first step of flow visualisation was registered by the Nikon D90 camera in a range of 2° to 14° and in a Reynolds number up to approximately 2×10^4. The comparison between the hydrofoils at 2° angle of attack is represented in the figure 3.

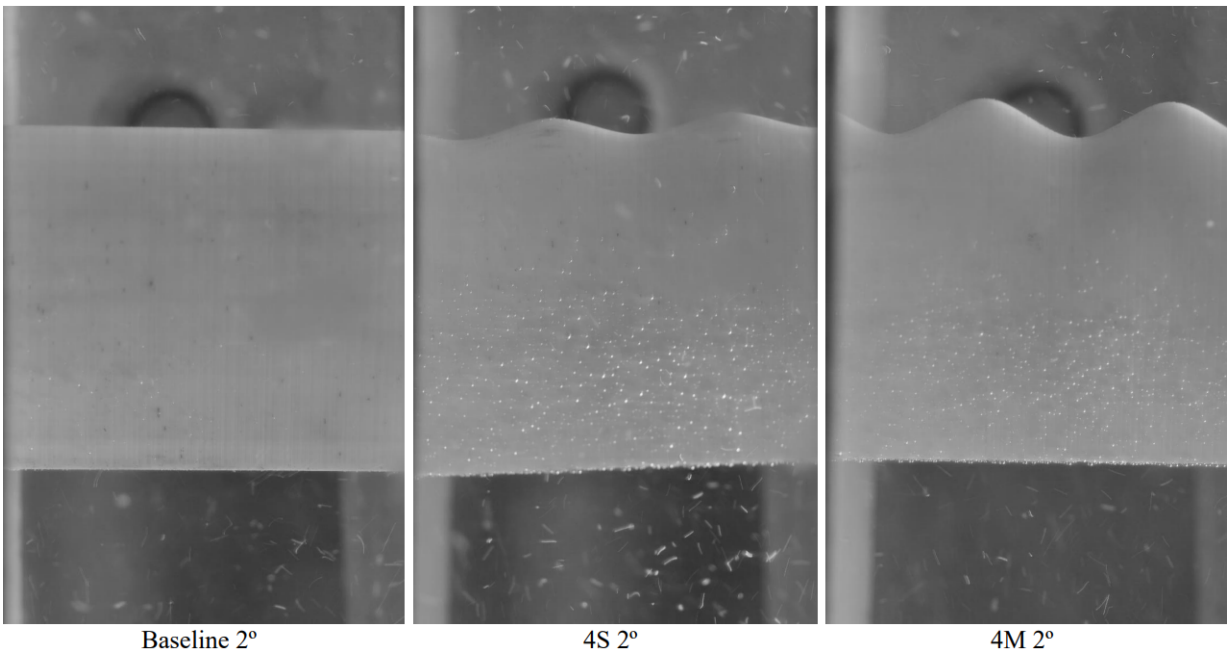

Figure 3. Flow visualisation of the hydrofoils at 2° angle of attack and Reynolds number of 8840. Developed by the authors.

It is noticeable in Figure 3 that the bubbles adhered in the modified hydrofoils are more expressive than in the baseline. On the other side, the bubbles in the fluid are similar in the all cases.

The comparison between the flows for the angle of attack of 8° showed interesting results that can be seen in the Figure 4 that show the flow in each hydrofoil with a Reynolds number of 5615. The bubbles can be seen in the baseline and in the 4M, while in the 4S there are no noticeable bubbles. Furthermore, the bubbles in the fluid in the case of the baseline are significantly more numerous than in the case of the 4M. Even with the increase in the Reynolds number, the appearance of notable bubbles in the 4S did not occur, as can be seen in Figure 5.

In the case of baseline and 4M, the images show bubble formation in both, but in the baseline the bubbles were significantly larger and were predominantly in the fluid. In the 4M the bubbles increased and were adhered to the foil. For Reynolds number greater than 11×10^3, in both cases, the bubbles in the fluid became expressive, hindering the visualisation in the photos.

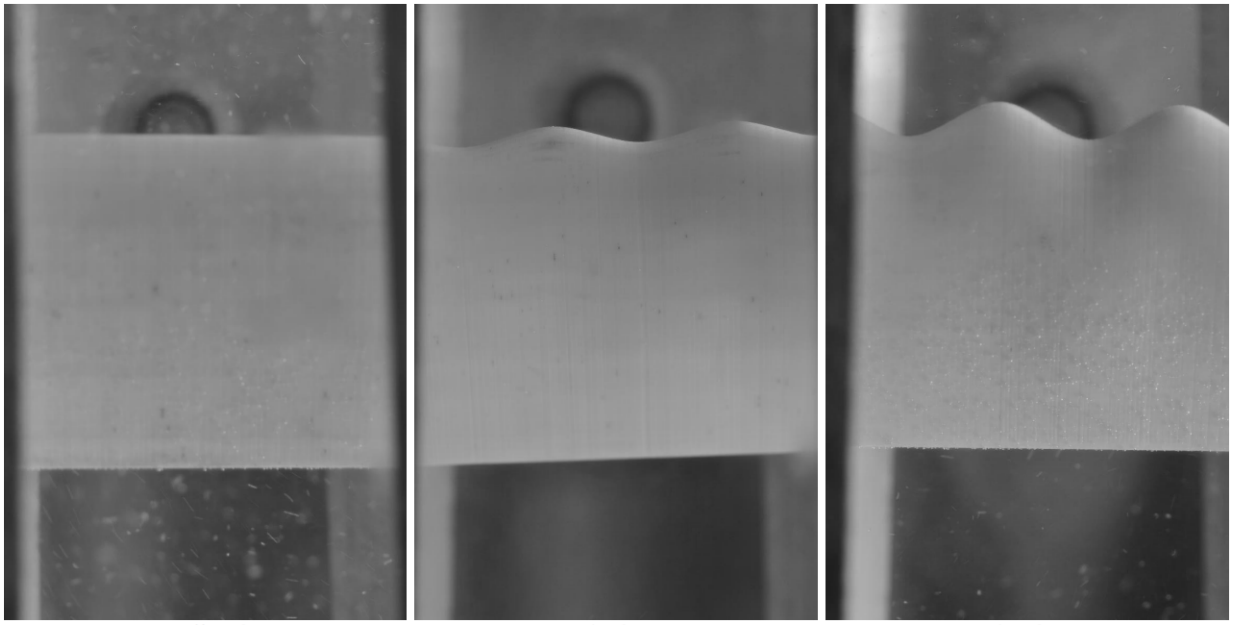

Figure 4. Flow visualisation of the hydrofoils at 8° angle of attack and Reynolds number of 5615. Developed by the authors.

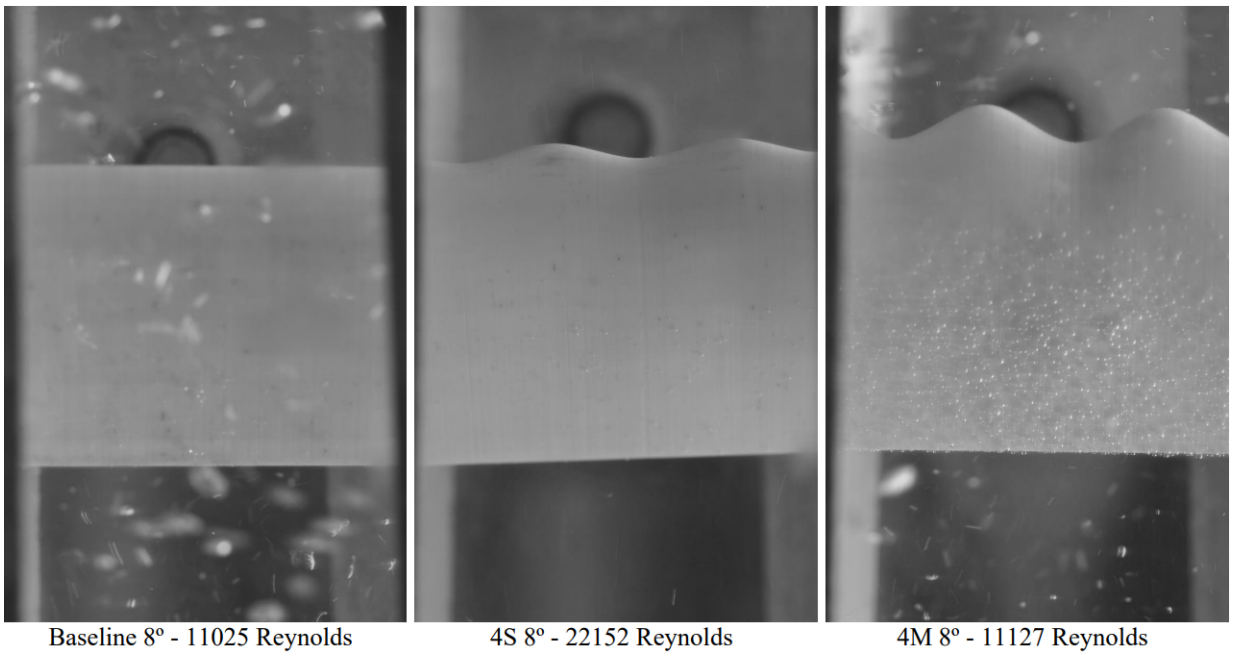

Figure 5. Flow visualisation of the hydrofoils at 8° angle of attack and increased Reynolds number. Developed by the authors.

At 14° angle of attack, the 3 foils provided very similar results, as can be seen in Figure 6, in which bubbles formed for a Reynolds number of approximately 3650.

So, with these flow visualisation results (Figures 3, 4 and 6), it was verified that, with the exception of the conditions in which the 4S did not present bubbles, there is a tendency for bubbles to appear in lower Reynolds numbers with increasing of the angle of attack.

The results shown in Figures 4 and 5 indicate that an 8° angle of attack is a favourable setup to reduce the appearance

of bubbles. This reduce indicates that the protuberances perform better in this angle, mainly the 4S. So, to a better understanding of the observed phenomenon, the tests with the high-speed camera were directed on these conditions that showed favourable results. Then, the hydrofoils were tested again at 8° angle of attack and with the same procedure, but with the high-speed camera.

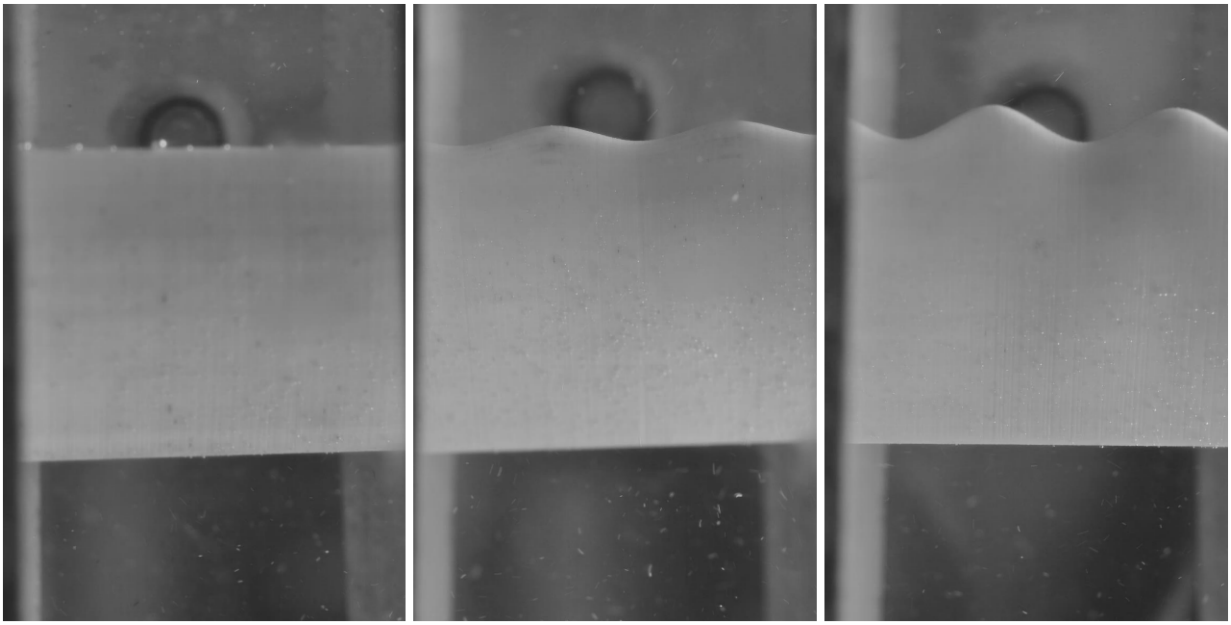

Baseline 14º 4S 14º 4M 14º

Figure 6. Flow visualisation of the hydrofoils at 14° angle of attack and Reynolds number of 3650. Developed by the authors.

In the Figures 7, 8 and 9, a frame, respectively, of the baseline, 4S and 4M is represented under a flow with the same conditions as in the Figure 4 (Reynolds number of approximately 5600 and angle of attack of 8°). But, differently from Figure 4, the high-speed camera allowed a better detail of the image and, consequently, allowed a better phenomenon analysis.

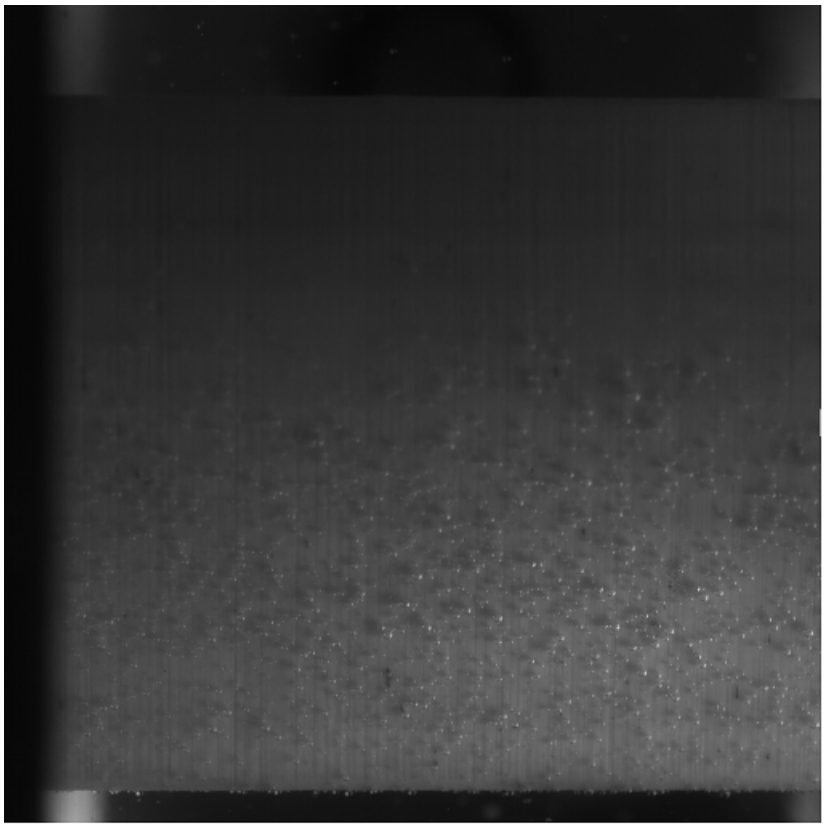

Figure 7. Baseline high-speed flow visualisation at 8° angle of attack and Reynolds number of 5600. Developed by the authors.

The comparison between the high-speed camera images confirms the previous analysis, as the baseline (Figure 7) notably has a very expressive amount of bubbles adhered to the hydrofoil and such bubbles are homogeneously distributed in a significant area of the trailing edge. The 4S (Figure 8), on the other hand, does not have any bubbles adhered to its surface again. And the 4M (Figure 9) has fewer bubbles than baseline. A possible explanation for this results is discussed by Li *et al.* (2021b), who concluded that protuberances act as vortex generators, influencing the vorticity in the boundary layer, improving the hydrodynamics of the hydrofoil and weakening the scale of cavitation. Thus, despite the different methodology, the results obtained by the authors have similarity with the results of this work, because the protuberances tend to reduce the cavitation too. So, plausibly, the 4S and 4M protuberances generate vortex that affect the boundary layer, which mitigate the adherence and the cavitation in some conditions. But, it is more noticeable in the 4S.

Agreeing with Custodio *et al.* (2018), the results obtained indicate that with the increase of the angle, there is a tendency to appear bubbles in lower numbers of Reynolds. Moreover, the main finding obtained by using the high-speed camera was the understanding of the origin of the bubbles adhered to the hydrofoils, because the appearance of bubbles is very dynamic to be recorded by the Nikon D90 camera. The high-speed camera's pictures indicate that the bubbles form in the fluid volume and adhere to the foil. After adhering to the foil's surface, the coalescence of the bubbles constantly occurs, thus, they become bigger until they detach from the foil. This conclusion can be seen in the Figure 10 where the coalescence is observed on a sequence of 3 frames, the frame 1 has three bubbles next to each other (highlighted section), after $1 \times 10^{-}3$ seconds there are 2 bubbles as can be seen in the frame 2. And, after more $1 \times 10^{-}3$ seconds, there is only one resulting bubble as consequence of the coalescence.

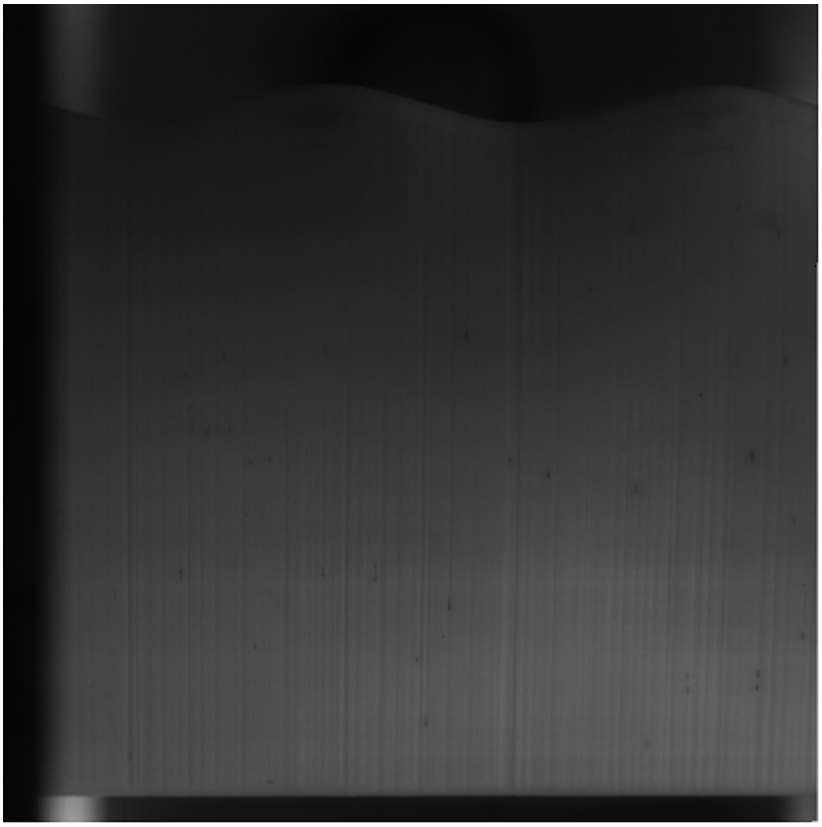

Figure 8. 4S high-speed flow visualisation at 8° angle of attack and Reynolds number of 5600. Developed by the authors.

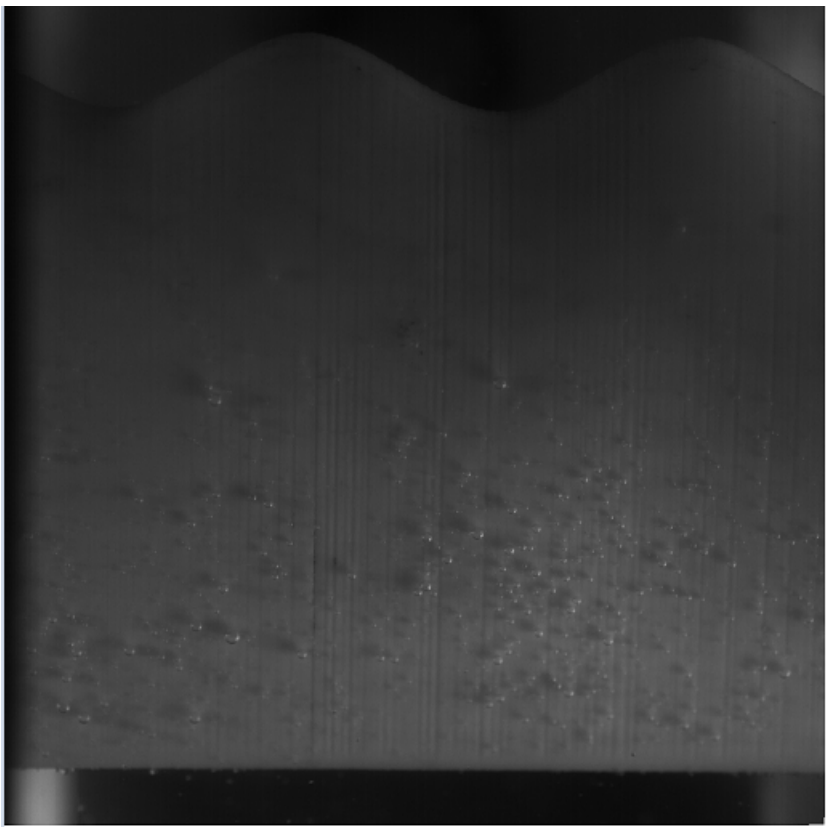

Figure 9. 4M high-speed flow visualisation at 8° angle of attack and Reynolds number of 5600. Developed by the authors.

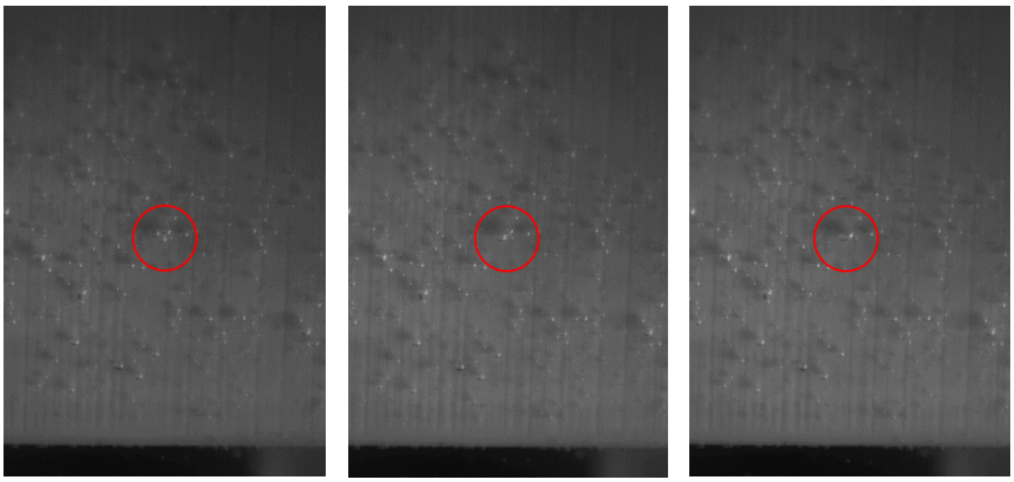

Figure 10. Bubbles coalescence. Developed by the authors.

4. CONCLUSIONS

In general, about the flow visualisation with the Nikon D90 camera, differences were noted in the flows of each hydrofoil in most conditions, but not necessarily the significant reduction of the bubbles, as in the case of 2° of attack angle in which modified hydrofoils have a significant amount of bubbles on the trailing edge while the baseline does not. For a 14° attack angle, there were no remarkable differences between the foils. With an attack angle of 8°, a reduction in the appearance of bubbles in modified profiles compared to baseline was recorded. The 4M presented some bubbles in its surface, but less than the baseline. The 4S presented some bubbles only in the flow, with no adherence to the profile. Therefore, there is a possibility of mitigating cavitation on 8° angle with modified profiles, especially the 4S, whose the protuberances performed better, avoiding the adherence.

The bubbles, probably, are originated in the TS section, because the structure of the test section (Figure 2) with the profile inside generates the Venturi effect. The narrowing caused by the profile and tunnel wall causes a speed increase and, consequently, a pressure drop, which is favourable to the incipient cavitation. So, probably, the bubbles are generated by this effect, but it is complex to check if the bubbles form first next to foil or in the volume of fluid. With the high-speed camera, a large amount of data was obtained, enabling a better analyse. So, tend to confirm that the bubbles originate in the fluid and then adhere to the profile. After the adhesion, it occurs coalescence in milliseconds and the bubbles increase in size (Figure 10), becoming remarkable and later detaching from the profile. The results presented may be used as a benchmark in numerical research.

5. ACKNOWLEDGEMENTS

This work has been possible in function of the São Paulo Research Foundation (FAPESP) grants, processes 2019/07947-0 (Regular Process) and 2021/08401-0 (Scientific Initiation).

6. REFERENCES

Bassan, R., 2011. *Visualização experimental de escoamentos no interior de canais munidos de protuberâncias parietais*. Master's thesis.

Custodio, D., Henoch, C. and Johari, H., 2018. "Cavitation on hydrofoils with leading edge protuberances". *Ocean Engineering*, Vol. 162, pp. 196–208.

Fish, F. and Battle, J., 1995. "Hydrodynamic design of the humpback whale flipper". *Journal of Morphology,225, 51- 60.*

Hansen, K.L., Rostamzadeh, N., Kelso, R.M. and Dally, B.B., 2016. "Evolution of the streamwise vortices generated between leading edge tubercles". *Journal of Fluid Mechanics*, Vol. 788, pp. 730–766.

Johari, H., 2015. "Cavitation on hydrofoils with sinusoidal leading edge". In *Journal of Physics: Conference Series*. IOP Publishing, Vol. 656, p. 012155.

Johari, H., Henoch, C., Custodio, D. and Levshin, A., 2007. "Effects of leading-edge protuberances on airfoil performance". *AIAA journal*, Vol. 45, No. 11, pp. 2634–2642.

Li, D., Yang, Q., Yang, W., Chang, H. and Wang, H., 2021a. "Bionic leading-edge protuberances and hydrofoil cavitation". *Physics of Fluids*, Vol. 33, No. 9, p. 093317.

Li, J., Liu, C. and Li, X., 2021b. "Effects of wavy leading-edge protuberance on hydrofoil performance and its flow

mechanism". *Journal of Marine Science and Engineering*, Vol. 9, No. 10, p. 1138.

Li, Z., Qian, Z. and Ji, B., 2020. "Transient cavitating flow structure and acoustic analysis of a hydrofoil with whalelike wavy leading edge". *Applied Mathematical Modelling*, Vol. 85, pp. 60–88.

Lindquist, C., 1999. "Estudo numérico e experimental do escoamento ao redor de cilindros de base quadrada e retangular".

Van Nierop, E.A., Alben, S. and Brenner, M.P., 2008. "How bumps on whale flippers delay stall: an aerodynamic model". *Physical review letters*, Vol. 100, No. 5, p. 054502.

7. RESPONSIBILITY NOTICE

The authors are solely responsible for the printed material included in this paper.